University of Zurich[UZH]

**Zurich Open Repository and Archive**
University of Zurich
University Library
Strickhofstrasse 39
CH-8057 Zurich
www.zora.uzh.ch

Year: 2012

# Regional forest and non-forest mapping using Envisat ASAR data

Ling, Feilong ; Li, Zengyuan ; Chen, Erxue ; Huang, Yanping ; Tian, Xin ; Schmullius, Christina ; Leiterer, Reik ; Reiche, Johannes ; Santoro, Maurizio

Abstract: Envisat Advanced Synthetic Aperture Radar (ASAR) dual-polarization data are shown to be effective for regional forest monitoring. To this scope, an automatic SAR image preprocessing procedure was developed using SRTM DEM and Land- sat TM image for geocoding in rugged terrain and smooth terrain areas, respectively. An object-oriented forest and non-forest classif ication method was then proposed based on the HH (horizontal transmit and horizontal receive) to HV (horizontal transmit and vertical receive) polarization intensity ratio and HV images of ASAR data at single acquisition time in winter. The developed method was applied to forest and non-forest mapping in Northeast China. The overall accuracy, the user's accuracy and the pro- ducer's accuracy of forest were 83.7%, 85.6% and 75.7%, respectively. These results indicate that the proposed method is prom- ising for operational forest mapping at regional scale.

Posted at the Zurich Open Repository and Archive, University of Zurich
ZORA URL: https://doi.org/10.5167/uzh-75142
Journal Article
Published Version

Originally published at:
Ling, Feilong; Li, Zengyuan; Chen, Erxue; Huang, Yanping; Tian, Xin; Schmullius, Christina; Leiterer, Reik; Reiche, Johannes; Santoro, Maurizio (2012). Regional forest and non-forest mapping using Envisat ASAR data. Yaogan Xuebao, 16(5):1101-1114.

# Regional forest and non-forest mapping using Envisat ASAR data

**LING Feilong[1], LI Zengyuan[2], CHEN Erxue[2], HUANG Yanping[1], TIAN Xin[2], SCHMULLIUS Christina[3], LEITERER Reik[3], REICHE Johannes[3], SANTORO Maurizio[4]**

1. *Key Laboratory of Spatial Data Mining & Information Sharing of Ministry of Education*, *Fuzhou University*, *Fuzhou*, 350002, *China*;
2. *Institute of Forest Resources Information Techniques*, *Chinese Academy of Forestry*, *Beijing*, 100091, *China*;
3. *Department of Earth Observation*, *Friedrich-Schiller University Jena*, *Jena*, 07745, *Germany*;
4. *Gamma Remote Sensing*, 3073 *Gümligen*, *Switzerland*

**Abstract:** Envisat Advanced Synthetic Aperture Radar (ASAR) dual-polarization data are shown to be effective for regional forest monitoring. To this scope, an automatic SAR image preprocessing procedure was developed using SRTM DEM and Landsat TM image for geocoding in rugged terrain and smooth terrain areas, respectively. An object-oriented forest and non-forest classification method was then proposed based on the HH (horizontal transmit and horizontal receive) to HV (horizontal transmit and vertical receive) polarization intensity ratio and HV images of ASAR data at single acquisition time in winter. The developed method was applied to forest and non-forest mapping in Northeast China. The overall accuracy, the user's accuracy and the producer's accuracy of forest were 83.7%, 85.6% and 75.7%, respectively. These results indicate that the proposed method is promising for operational forest mapping at regional scale.

**Key words:** Envisat ASAR, forest mapping, object-oriented classification, Northeast China

**CLC number:** TP79 **Document code:** A

**Citation format:** Ling F L, Li Z Y, Chen E X, Huang Y P, Tian X, Christina S, Reik L, Johannes R and Maurizio S. 2012. Regional forest and non-forest mapping using Envisat ASAR data. Journal of Remote Sensing, 16(5): 1101–1114

## 1 INTRODUCTION

Forests are dominant biomes of the earth and have important impacts on economic and environmental well-being. Because of the timely and continuous earth observation capability, remote sensing satellites are beneficial for the understanding of forest status. The usefulness of optical satellite remote sensing is limited by cloudy weather conditions and reduced solar illumination. Synthetic aperture radar (SAR), instead, can ensure data acquisition owing to the independence on weather conditions and sun angle (Henderson & Lewis, 1998). Satellite SAR data have been used for forest mapping at regional scale in boreal forest (Schmullius, et al.,1999; Baker, et al., 2001; Wagner, et al., 2003; Rosenqvist, et al., 2004; Rauste, 2005), tropical forest (De Grandi, et al., 2000), and globally regions (Shimada, et al., 2011). For the monitoring of forest of Northeast China, Cartus, et al. (2011), proposed a forest growing stock volume estimation method based on European Remote Sensing ERS-1/2 tandem coherence and produced a forest growing stock volume map for Northeast China, using data acquired during 1995 and 1996. Compared to ERS-1 and ERS-2, the Envisat Advanced Synthetic Aperture Radar (ASAR), launched in 2002, has additional features, such as multi-incidence angles and multi-polarization imaging capabilities. In particular, the Alternative Polarization (AP) mode can acquire data with two polarizations simultaneously (HH/VV, HH/HV or VV/VH).

The objective of this paper is to develop a regional forest and non-forest mapping method based on Envisat ASAR Alternative Polarization mode data at a single acquisition. The approach has been applied to produce a forest and non-forest map for Northeast China for 2005.

## 2 TEST SITE AND DATA

### 2.1 Geographic area

Northeast China, covers 1.26 million km$^2$, 13% of China's total acreage, and includes eastern Inner Mongolia Autonomous Region,

**Received:** 2011-09-30; **Accepted:** 2012-03-02

**Foundation:** National Basic Research Program (973 Program) (No.2007CB714404); Fujian Science Project (No.200910014)

**First author biography:** LING Feilong (1977— ), male, Ph.D., research assistant. His research interests are radar remote sensing applications to forestry and agriculture. E-mail: lfl@fzu.edu.cn

**Corresponding author biography:** LI Zengyuan (1959— ), male, Ph.D., professor. His research interests are related to radar remote sensing with applications to forestry. E-mail: lizy@caf.ac.cn

the Heilongjiang province, the Jilin province and the Liaoning province. Climate of this area is temperate monsoon, with winter lasting more than half a year and precipitation concentrated in summer. The main forest areas in Northeast China are in Daxinganling, Xiaoxinganling and Changbaishan. The growing stock volume of Northeast China accounts for 1/3 of China's total forest stock volume.

### 2.2 Reference data

For geocoding of the SAR data, 90 m Shuttle Radar Topography Mission (SRTM) Digital Elevation Model (DEM) resampled to 100 m was used.

For geocoding of the ASAR images in flat terrain areas and for validation of the mapping results, we used a Landsat TM dataset of 2005 and the derived land use map for Northeast China. This land use map, with 30 m spatial resolution, has 10 thematic classes-conifer forest, broad leaf forest, mixed forest, shrub, agricultural field, high density grassland, grassland, water, urban and a class named other. In terms of forest and non-forest, this map has an overall accuracy of 83%, which is validated with the national forest inventory dataset of Jilin province. To use this land use map to validate our result, we combined the three forest classes and shrub into forest and the remainder into non-forest.

### 2.3 SAR data

More than 900 multi-temporal ASAR images acquired between July 2004 and March 2005 were available for this study. The data were acquired in the Alternating Polarization mode along descending orbits (10 a.m. Local time). All images were acquired at nominal incidence angle of 23° and with HH/HV polarization. The ground range spatial resolution of the images is approximately 30 m, whereas the data were provided with a sampling of 12.5 m.

## 3 DATA PREPROCESSING

Data preprocessing consists of calibration, multi-looking, speckle filtering, ratio image computation, geocoding and radiometric terrain correction. The images were calibrated using the calibration constant provided by the European Space Agency. To obtain the output pixel size of 50 m, images were averaged with multi-looking factors of 4 both in range and azimuth.

### 3.1 Image filtering

Filtering for speckle noise is necessary to avoid errors during the image segmentation and classification. To reduce speckle noise while preserving the spatial resolution, we used multi-channel filtering (Quegan & Yu, 2001), which makes full use of the HH and HV information of the data. A Lee filter with 3×3 window was used to further reduce the speckle (Lee, 1980).

### 3.2 Ratio image

Although the polarimetric ratio image $\hat{r}$ between two images acquired with different polarizations is a useful feature for classification and can suppress topographic effects on the SAR backscatter, it is more sensitive to speckle noise than either of the single image used for ratio computation. Therefore, we computed the ratio using the average values within a spatial window

$$\hat{r} = \frac{\frac{1}{M}\sum_{i=1}^{M} I_{\mathrm{HH},i}}{\frac{1}{M}\sum_{i=1}^{M} I_{\mathrm{HV},i}} \tag{1}$$

where $I_{\mathrm{HH},}i$ and $I_{\mathrm{HV},}i$ are the mean intensity values of HH and HV image in the estimation window with $M$ pixels.

### 3.3 Geocoding

To geocode the SAR images, a procedure based on a lookup table linking the radar and the map geometry was used (Wegmüller, 1999). The lookup table is generated from orbital information and the SRTM DEM. Such data is also used to produce a simulated SAR image, which helps to identify ground control point (GCPs) to quantify possible offsets between the true map geometry and the geometry described in the lookup table. GCPs Correlation match between the SAR imagery and the corresponding simulated SAR imagery serves to identify the offsets. The estimate of the offsets is then used to refine the lookup table which is finally used to resample the SAR imagery from slant range geometry to map geometry.

Fig. 1 shows that, in rugged terrain areas, the simulated SAR image is similar to the real SAR image, thus being suitable for the selection of GCPs. By comparison, Fig. 2 shows that for predominantly flat terrain, the simulated SAR image does not contain features that can be used as GCPs. In contrast, the red band of Landsat TM data (Fig. 2) and the SAR image have many thematic features in common, such as urban areas, roads and water bodies. In such cases, these common features are good candidates of GCPs for geocoding. An optical image can therefore be used instead of the simulated SAR image from the DEM.

Fig. 3 shows the procedure implemented for geocoding the Envisat ASAR images. First, the orbit data and SRTM DEM were used to create a simulated SAR image. Second, GCPs were selected by correlation match between SAR and simulated SAR images. Third, the correlation match result was evaluated. If the number of GCPs was less than 20 or standard deviation of the GCP fit was over 0.4 (fraction of a pixel), the Landsat TM image, instead of the

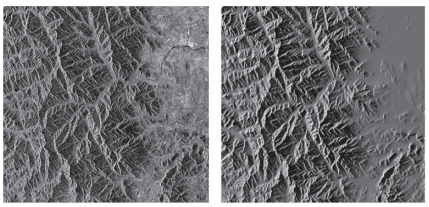

(a) SAR image (b) Simulated SAR image

Fig. 1 SAR and simulated SAR image for rugged terrain area

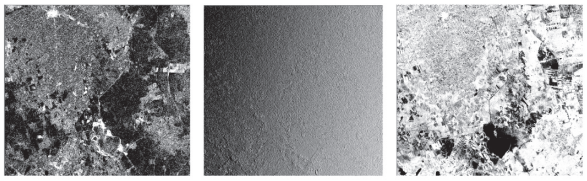

(a) SAR image (b) Simulated SAR image (c) Landsat TM image

Fig. 2 Images for flat terrain area

simulated SAR image, was used to identify GCPs through correlation match again. Finally, a lookup table that provided the transfer function between the slant-range and map geometry was produced based on the bilinear fit of the offset estimates in correspondence of the GCPs. The geocoding was finally carried out with this lookup table. The accuracy of the geocoding was within one pixel. The whole processing was completely automated based on the Gamma software commands and Unix script language.

All SAR images were geocoded to the Albers Conical Equal Area coordinate system with an ellipsoid defined by WGS84. The central longitude is 130°E. The two parallel lines are 47°N and 25°N. The SAR images were geocoded to a pixel size of 50 m.

Fig. 4 shows the geocoded color composite ASAR mosaic of Northeast China, with the backscattered intensity at HH-polarization in the red and the blue channels, and the backscattered intensity at HV-polarization in the green channel. Forests correspond to areas were shown in green. In contrast to other land surfaces in the study area characterized by surface scattering, forests are the only land cover with predominant volume scattering. The stronger HV backscattering coefficient in forests explains the green color for forests in Fig. 4.

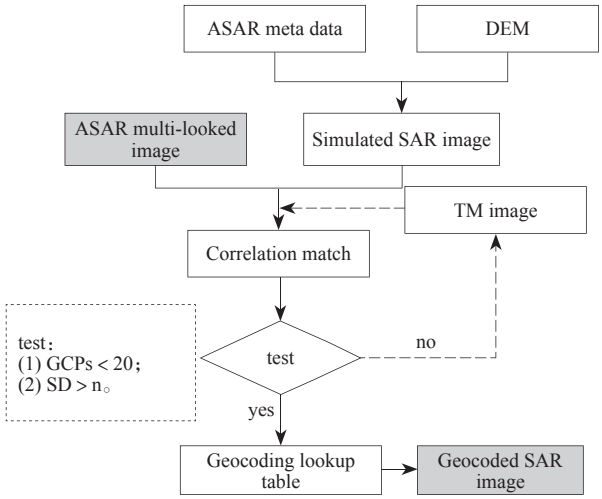


Fig. 3 Flowchart of procedure implemented for geocoding of the Envisat ASAR images

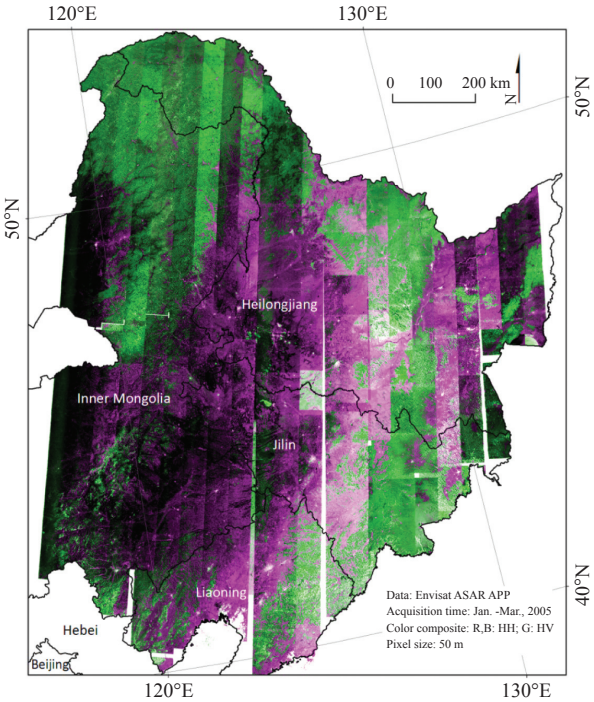


Fig. 4 Envisat ASAR mosaic of Northeast China (Data were acquired from January 2005 to March 2005; color composite: R and B: backscattered intensity, HH-polarization; G: backscattered intensity HV-polarization)

## 4 FOREST / NON-FOREST CLASSIFICATION

The selection of data and data features is important to the classification accuracy. Therefore, we made analysis to determine the optimum SAR data acquisition time and the optimum data features as inputs for the classification algorithm. An object based hierarchical classification algorithm was then developed based on the analysis. eCognition software was used for the automation of the classification.

### 4.1 Data analysis

Image features, such as texture, polarimetric intensity ratio, geometric feature and relationship between the segmented image objects, can be derived from the original HH and HV images of Envisat ASAR data. The analysis was first performed by means of the eCognition software's Feature Space Optimization tool, which evaluated all the data features. The feature space optimization tool, together with visual comparison between different image features, showed that the polarimetric ratio between HH and HV intensity images was the best feature.

The Envisat ASAR data available can be divided to summer data (July 2004—October 2004) and winter data (December 2004—March 2005). Fig. 5 shows an example of comparison between summer and winter data. The winter backscatter ratio appeared to yield the best separation between forest and non-forest since it presented the greatest contrast. The environmental conditions in winter are characterized by low temperatures below the freezing point and snow cover. Agricultural fields are bare. Summer data instead showed little forest / non-forest contrast because of the higher soil moisture due to precipitation and the presence of crops. Fig. 5 shows that mostly cropland presents similar signatures compared to forest. Fig. 5(f) shows greater contrast between forest and non-forest for HV-polarization data than Fig. 5(b). While both forest and crops are green in the summer color composite (Fig. 5(d)), only forest is green in the winter color composite (Fig. 5(h)).

Fig. 6 shows the histograms of the data shown in Fig. 5. Fig. 6(a), Fig. 6(c) and Fig. 6(e) show that none of the summer HH, summer HV and summer ratio can separate forest from cropland. Fig. 6(f) shows that winter ratio is best indicator for forest/non-forest discrimination. Water bodies, such as lakes and rivers, can also be separated from forest by the winter ratio image, although water bodies presented strong backscattering because of the increased surface roughness and volume scattering due to snow and ice cover.

Visual comparison and histogram analysis show that winter data are more suitable for forest and non-forest classification than summer data, and that polarimetric intensity ratio is more suitable for forest / non-forest classification compared to HV-backscatter and

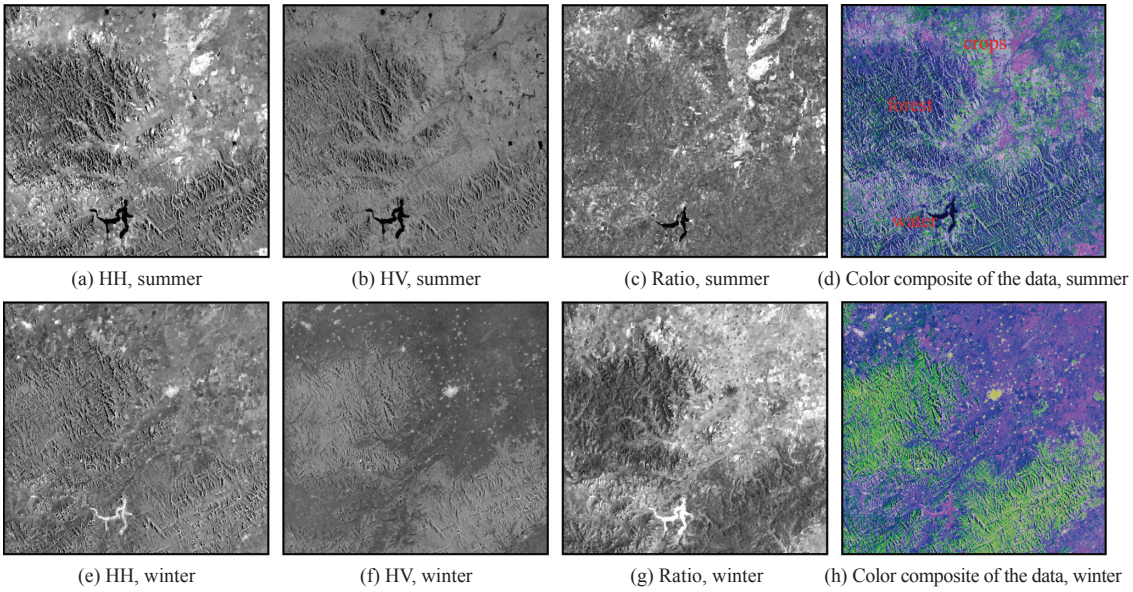


(a) HH, summer (b) HV, summer (c) Ratio, summer (d) Color composite of the data, summer

(e) HH, winter (f) HV, winter (g) Ratio, winter (h) Color composite of the data, winter

Fig. 5 Comparison between summer and winter ASAR data (summer: 2004-09-04; winter: 2005-02-26)
(Red:HH; Green:HV; Blue:ratio)

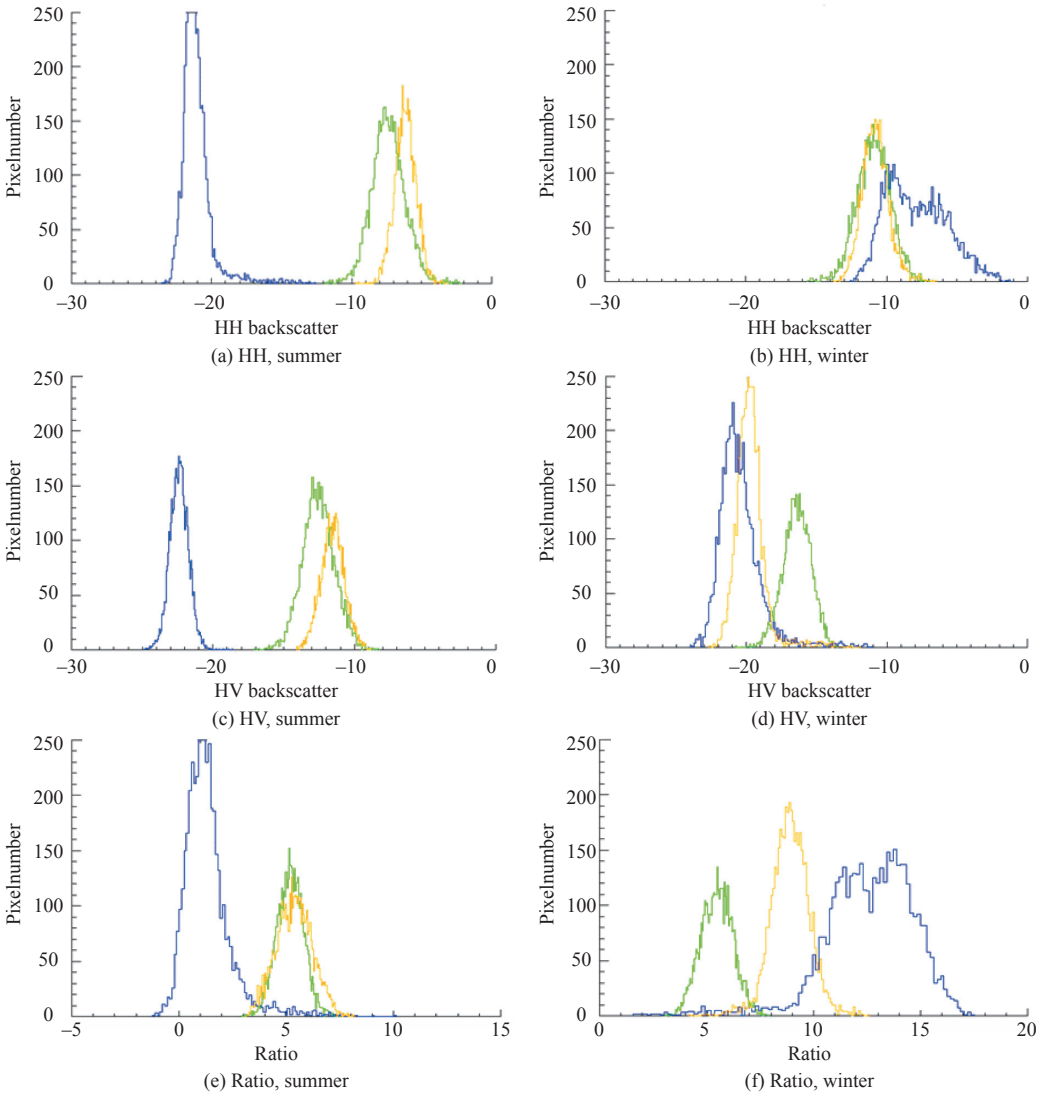


(a) HH, summer (b) HH, winter

(c) HV, summer (d) HV, winter

(e) Ratio, summer (f) Ratio, winter

Fig. 6 ASAR histograms of the typical land covers

HH-backscatter. In addition, we found that some vegetation types have similar low ratio values as that of forest, for example, the high density grassland in Inner Mongolia. However, this grassland vegetation has very low HV value, which is different from that of forest. Therefore, we used both polarimetric intensity ratio and the HV-backscatter image of the winter acquisitions (January 2005 - March 2005) as inputs for the following classification algorithm for forest and non-forest mapping in Northeast China.

### 4.2 Object oriented classification

Fig. 7 shows the developed hierarchical classification method based on the ratio image and the HV-backscatter image of winter ASAR data. The eCognition-based method consists of image segmentation, object based classification and classification result optimization.

First, the multi-resolution segmentation method (Benz, et al., 2004) was used for image segmentation. Three parameters determine the results of the multi-resolution segmentation: scale, color and shape. The scale parameter determines the maximum allowed heterogeneity for the resulting image objects; the higher the value, the larger the resulting image objects. The object homogeneity to which the scale parameter refers is defined by the color parameter and the shape parameter. In most cases, the color criterion is the most important for creating meaningful objects, whereas the shape parameter can help to avoid highly fractured image object results in strongly textured data. Our goal is to make the segmented image objects as large and homogenous as possible. After trying different parameters, we used 10 as scale parameter, 0.9 as color parameter and 0.1 as shape parameter, mainly based on visual interpretation.

Then, a hierarchical classification was performed based on the segmented image objects. Object oriented classification can use not only the backscatter intensity information of the image but also the relationship between the objects. The first step of the classification with eCognition is to separate the image area from the background area with two rules: (1) HV mean object values equal to 0 for class Background;(2) the inverted similarity to Background objects was used for class Image area. The second step is to separate forest from non-forest within the Image area with the help of the class inheritance capability of eCognition. The dynamic ranges of both ratio and HV intensity for forest were used to set the classification rules for class Forest; the inverted similarity to Forest was then used to classify Non-Forest objects. The thresholds shown in Fig. 7 varied a little according to different strips at different acquisition time. Finally, the relationship between the objects was used to optimize the initial classification. The initial classification included many small and discrete objects, for example, a forest object surrounded by continuous non-forest objects, or vice versa. The discrete classified objects were caused by two factors. One is the geometric and radiometric distortions due to topography in mountainous areas; the other is discretely distributed trees and other vegetation that have similar radar backscattering as that of forest. Two rules were set for the initial classification optimization: (1) reclassify a Non-Forest object to Forest when more than 80% of this Non-Forest object's border is adjacent to the borders of the surrounding Forest objects; (2) reclassify a Forest object to Non-Forest when more than 80% of this Forest object's border is adjacent to the borders of the surrounding Non-Forest objects. This optimization not only made the classification map smoother than the initial by merging the small and discrete objects, but also classified the objects of foreshortening and layover. The automation of the classification process shown in Fig. 7 was realized by eCognition's Processing Tree tool.

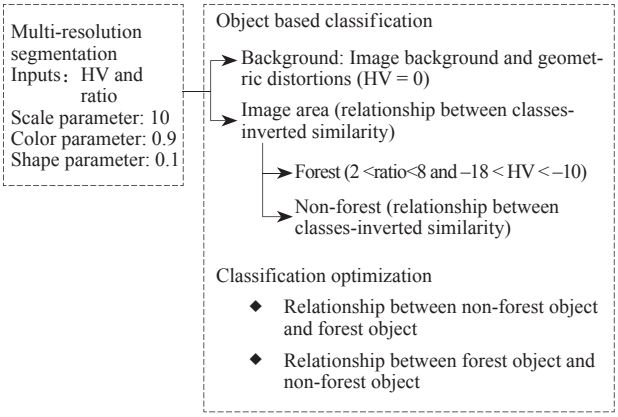


Fig. 7 Flow chart of object based forest and non-forest classification using ENVISAT ASAR data

## 5 RESULT AND ERROR ANALYSIS

### 5.1 Classification result

Fig. 8 shows the forest and non-forest map of Northeast China derived from Envisat ASAR winter data of 2005. Table 1 shows the classification accuracy referring to the Landsat TM land use map. The accuracy measurement was based on the error matrix (Congalton, 1991; Foody, 2002). The Kappa coefficient is a measure for the reliability between the classification and the reference data, and to estimate the random effect of the classification result. The over-

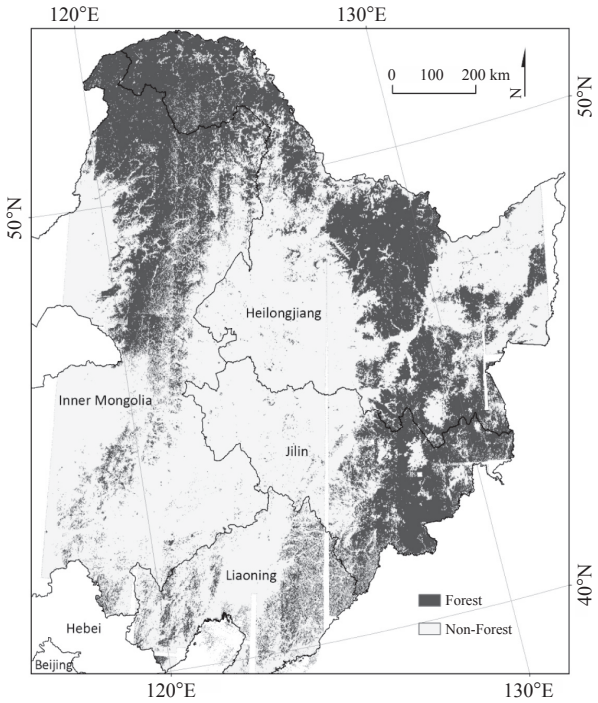


Fig. 8 Forest and non-forest map of Northeast China from ENVISAT ASAR data

all accuracy is calculated by dividing the correctly classified pixels by the total number of pixels. The producer's accuracy is derived by dividing the number of correct pixels in one class divided by the total number of pixels as derived from reference data. The higher errors of omission exist, the lower the producer's accuracy. If the correct classified pixels in a class are divided by the total number of pixels that are classified in that class, this measure is called user's accuracy. The higher errors of commission exist, the lower the user's accuracy.

**Table 1 Classification accuracy of forest and non-forest map of Northeast China**

| Kappa index | Overall accuracy | Forest user's accuracy | Forest producer's accuracy | Non-forest user's accuracy | Non-forest producer's accuracy |
|---|---|---|---|---|---|
| 0.67 | 83.7% | 85.6% | 75.7% | 82.6% | 90% |

## 5.2 Error analysis

Northeast China covers a large geographic area with various topography and different landscapes. The Envisat ASAR data were acquired at different times and under different meteorological conditions. The different environmental conditions under which the Envisat ASAR data were acquired complicated the use of one classification method to all the data. Fig. 9 shows the classification error map based on the Landsat TM land use map. The commission error of the class "forest" was due to crop field and grassland. For example, the forest tree nursery, located in area A in Fig. 9 in purple, was misclassified as forest due to similar backscattering. Area B in Fig. 9 shows another example of commission error for the class "forest" (the red area); this area was grassland in 2005 and recovered from a large forest fire that occurred in 2003. In some burned areas, however, some trees survived which implied that the area was misclassified as forest. Omission errors, i.e., forest areas misclassified as non-forest, were more significant than commission errors, which is shown by the large blue area in Fig. 9 and the low producer's accuracy of forest in Table 1. The omission of forest was primarily caused by terrain variations. The blue strips, along the azimuth direction in area C in Fig. 9, showed the problem of terrain variation and local incidence angle, causing the lower classification accuracy in the image near range than the accuracy in the far range. Omission of forest also occurred in area D and E, which are typical broken terrain with great variations.

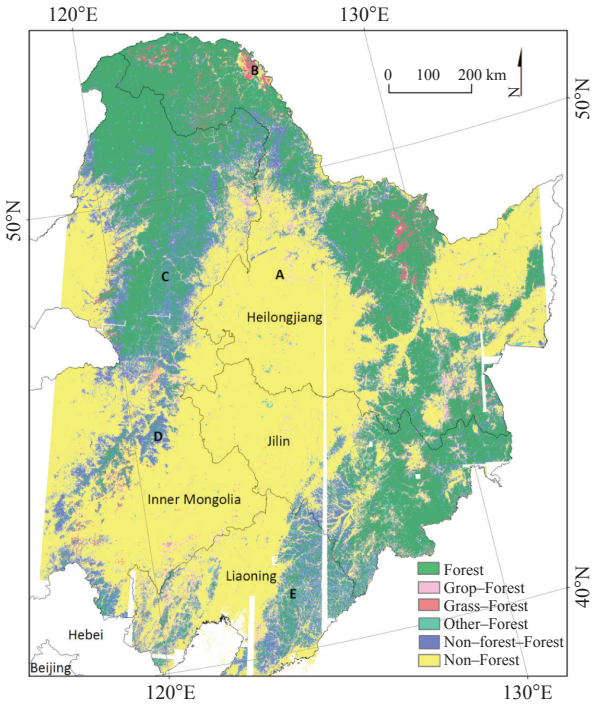


Fig. 9 ASAR forest and non-forest classification error map

The accuracy of the reference map used for validation should be considered for error analysis. Our field visit to Mohe county, in September 2011, confirmed that some areas labeled as grassland in the Landsat TM land use map were changed to forest in 2005; this indicate that the ASAR derived forest and non-forest map is correct in some areas, while the reference dataset presented some errors.

# 6 CONCLUSION

An automatic SAR data processing method and an object based forest and non-forest classification method were developed based on the ENVISAT ASAR HH/HV mode data. Satisfactory mapping accuracy was achieved when the methods were used for regional forest and non-forest mapping in Northeast China. The proposed methods are effective in timely and accurate regional forest and non-forest mapping.

# REFERENCES

Baker J, Balzter H, Davidson M, Eriksson L, Gaveau D, Gluck M, Holz A, Luckman A, Marschalk U, McCallum I, Nilsson S, Öskog A, Quegan S, Rauste Y, Roth A, Schmullius C, Shvidenko A, Tansey K, Le Toan T, Vietmeier J, Wagner W, Wegmüller U, Wiesmann A and Yu J J. 2001. SAR Imaging for Boreal Ecology and Radar Interferometry-Final report. [2011-05-02] http://www.siberia1.uni-jena.de/

Benz U C, Hofmann P, Willhauck G, Langenfelder I and Heynen M. 2004. Multi-resolution, object-oriented fuzzy analysis of remote sensing data for GIS-ready information. ISPRS Journal of Photogrammetry and Remote Sensing, 58(3/4): 239–258 [DOI: 10.1016/j.isprsjprs.2003.10.002]

Cartus O, Santoro M, Schmullius C and Li Z Y. 2011. Large area forest stem volume mapping in the boreal zone using synergy of ERS-1/2 tandem coherence and MODIS vegetation continuous fields. Remote Sensing of Environment, 115(3): 931–943 [DOI: 10.1016/j.rse.2010.12.003]

Congalton R G. 1991. A review of assessing the accuracy of classifications of remotely sensed data. Remote Sensing of Environment, 37(1): 35–46 [DOI: 10.1016/0034-4257(91)90048-B]

De Grandi G, Mayaux P, Rauste Y, Rosenqvist A, Simard M and Saatchi S S. 2000. The Global Rain Forest Mapping Project JERS-1 radar

mosaic of tropical Africa: development and product characterization aspects. IEEE Transactions on Geoscience and Remote Sensing, 38(5): 2218–2233 [DOI: 10.1109/36.868880]

Foody G M. 2002. Status of land cover classification accuracy assessment. Remote Sensing of Environment, 80(1): 185–201 [DOI: 10.1016/S0034-4257(01)00295-4]

Henderson F M and Lewis A J. 1998. Principles and Applications of Imaging Radar, Manual of Remote Sensing, Third Edition, Volume 2. Toronto: ASPRS, John Wiley and Sons Inc

Lee J S. 1980. Digital image enhancement and noise filtering by use of local statistics. IEEE Transactions on Pattern Analysis and Machine Intelligence, 2 (2): 165–168

Quegan S and Yu J J. 2001. Filtering of multichannel SAR images. IEEE Transactions on Geoscience and Remote Sensing, 39(11): 2373–2379 [DOI: 10.1109/36.964973]

Rauste Y. 2005. Multi-temporal JERS SAR data in boreal forest biomass mapping. Remote Sensing of Environment, 97(2): 263–275 [DOI: 10.1016/j.rse.2005.05.002]

Rosenqvist A, Shimada M, Chapman B, McDonald K, De Grandi G, Jonsson H, Williams C, Rauste Y, Nilsson M, Sango D and Matsumoto M. 2004. An overview of the JERS-1 SAR Global Boreal Forest Mapping (GBFM) project. Proceedings of 2004 IEEE International Geoscience and Remote Sensing Symposium, 2: 1033–1036

Schmullius C, Holz A and Vietmeier J. 1999. SIBERIA-results from the IGBP Boreal Forest Transect. Hamburg: Proceedings of IGARSS’99 Conference: 2118–2120 [DOI: 10.1109/IGARSS.1999.775049]

Shimada M, Isoguchi O, Motooka T, Shiraishi T, Mukaida A, Okumura H, Otaki T, Itoh T, Rosenqvist A, Kato A and Sasai T. 2011. Generation of 10 m resolution palsar and jers-sar mosaics and forest/non-forest maps for forest carbon monitoring. Proceedings of ISRSE34, Sydney, Australia

Wagner W, Luckman A, Vietmeier J, Tansey K, Balzter H, Schmullius C, Davidson M, Gaveau D, Gluck M, Le Toan T, Quegan S, Shvidenko A, Wiesmann A and Yu J J. 2003. Large-scale mapping of boreal forest in SIBERIA using ERS tandem coherence and JERS backscatter data. Remote Sensing of Environment, 85(2): 125–144 [DOI: 10.1016/S0034-4257(02)00198-0]

Wegmüller U. 1999. Automated Terrain Corrected SAR Geocoding. Hamburg: Proceedings of IGARSS’99: 1712–1714

# 基于ENVISAT ASAR的区域森林-非森林制图

凌飞龙[1]，李增元[2]，陈尔学[2]，黄燕平[1]，田昕[2]，Schmullius Christina[3]，Leiterer Reik[3], Reiche Johannes[3], Santoro Maurizio[4]

1. 福州大学 空间数据挖掘与信息共享教育部重点实验室，福建 福州 350002；
2. 中国林业科学研究院 资源信息研究所，北京 100091；
3. 德国耶拿大学 对地观测研究所；
4. 瑞士Gamma遥感公司

**摘 要**：Envisat卫星ASAR传感器的双极化数据对区域森林监测十分有效。通过分别采用SRTM DEM和Landsat TM图像对地形起伏区域和平坦区域的SAR图像进行地理编码，发展了一种SAR图像自动预处理方法。基于冬季单时相ASAR数据的HH(水平发射，水平接受)、HV(水平发射，垂直接收)极化比值和HV极化图像，提出了一种面向对象的森林-非森林分类方法。将之应用于中国东北森林/非森林制图，分类总体精度、森林用户精度和生产者精度分别为 83.7%，85.6%和75.7%。结果表明，本文提出的方法十分适合区域森林-非森林制图的业务化运行。

**关键词**：Envisat ASAR，森林制图，面向对象分类

**中图分类号**：TP79 **文献标志码**：A

引用格式：凌飞龙，李增元，陈尔学，黄燕平，田昕，Christina S, Reik L, Johannes R, Maurizio S. 2012. 基于ENVISAT ASAR的区域森林–非森林制图. 遥感学报，16(5): 1101–1114

Ling F L, Li Z Y, Chen E X, Huang Y P, Tian X, Christina S, Reik L, Johannes R and Maurizio S. 2012. Regional forest and non-forest mapping using Envisat ASAR data. Journal of Remote Sensing, 16(5): 1101–1114

## 1 引 言

森林是地球的优势生物群落，对全球经济和环境十分重要。遥感卫星能及时对地球进行周期性观测，有益于人们对森林状态的理解。光学传感器在云、雨天气条件下获取数据十分困难；雷达则较少受天气条件的影响，是遥感数据源有力的保证(Henderson和Lewis，1998)。

星载SAR数据已经被应用于大区域森林制图，例如SIBERIA–1&2(Schmullius 等，1999；Baker 等，2001；Wagner 等，2003)、全球热带雨林SAR遥感监测(De Grandi 等，2000)、全球北方森林SAR遥感监测(Rosenqvist 等，2004；Raust，2005)和ALOS PALSAR全球森林-非森林制图(Shimada 等，2011)。Cartus等人(2011)提出了基于ERS-1/2串行干涉数据反演森林蓄积量的方法，并使用1995年—1996年间的数据生产了中国东北森林蓄积量图。

相比于ERS-1和ERS-2 SAR，2002年投入运行的ENVISAT ASAR传感器具有多入射角和多极化等新特性。其中，交替极化成像模式可同时获取两种极化组合的数据(HH/VV、HH/HV或者VV/VH)。

本文旨在提出基于单时相ENVISAT ASAR交替极化数据的区域森林-非森林制图方法，并应用该方法制作2005年中国东北森林-非森林分布图。

## 2 研究区和数据

### 2.1 地理区域

中国东北地区包括内蒙古东部、黑龙江省、吉林省和辽宁省，土地面积为126万km$^2$，占全国国土面

**收稿日期**：2011-09-30；**修订日期**：2012-03-02

**基金项目**：国家重点基础研究发展计划 (973 计划) (编号: 2007CB714404); 福建省科技计划(编号: 200910014)；中欧合作“龙计划”项目(编号: 5314)

**第一作者简介**：凌飞龙(1977— )，男，博士，助理研究员。主要从事SAR遥感森林和农业应用研究。E-mail: lfl@fzu.edu.cn。

**通信作者简介**：李增元(1959— )，男，研究员。主要从事森林遥感相关领域的研究工作。E-mail: lizy@caf.ac.cn。

积的13%。东北地区地域广阔，气候类型多样，主要气候类型为温带季风气候,冬季长达半年以上，雨量集中于夏季。东北森林主要分布在大兴安岭、小兴安岭和长白山脉，占中国总森林蓄积量的1/3。

### 2.2 参考数据

获取了覆盖东北的90 m分辨率SRTM DEM数据，将其重采样成100 m，用于ASAR数据地理编码。

获取了2005年的Landsat TM数据及由其生成的土地利用图。该图具有针叶林、阔叶林、混交林、灌木、农田、高盖度草地、草地、水体、城镇建筑和其他类共10个类别，分辨率为30 m。利用同时期的吉林省国家森林资源一类调查数据进行验证，分类总体精度为83%。我们将前4个类别合并为森林，利用其对制图结果进行精度评价。

### 2.3 SAR数据

获取了2004年—2005年覆盖东北的多时相ASAR数据共900余景。成像模式为ENVISAT ASAR条带式扫描模式，中央入射角为23°，图像分辨率约30 m，幅宽100 km，极化方式为HH和HV组合，降轨成像。获取的地距图像采样间隔为12.5 m。

## 3 数据预处理

数据处理包括：辐射定标、多视处理、斑点滤波、极化比值运算、几何校正、地形辐射校正以及对数转换。根据ESA提供的定标常数对ENVISAT ASAR交替极化数据进行标定，采用4×4多视处理，处理后的图像采样间隔为50 m。

### 3.1 图像滤波

为降低图像分割与分类的误差，须对斑点噪声滤波。为了消除斑点噪声影响，又保持图像的分辨率，利用每一景图像的HH和HV两个极化波段进行多通道滤波(Quegan和Yu，2001)，再进行3×3窗口的Lee滤波进一步消除噪声(Lee，1980)。

### 3.2 比值计算

极化比值图像不仅是分类的有效波段，而且能消除地形影响。但比值图像$\hat{r}$比单一图像对斑点噪声更为敏感，本文采用在包含$M$个像元的空间窗口内进行计算的方法，如式(1)。

$$\hat{r}=\frac{\frac{1}{M}\sum_{i=1}^{M}I_{\mathrm{HH},i}}{\frac{1}{M}\sum_{i=1}^{M}I_{\mathrm{HV},i}} \tag{1}$$

式中，$I_{\mathrm{HH},i}$和$I_{\mathrm{HV},i}$分别代表辐射定标后第$i$个像元的HH和HV极化强度值。

### 3.3 地理编码

采用基于雷达几何与地图几何关系的查找表方法进行SAR图像的地理编码(Wegmüller，1999)。这一查找表由卫星轨道信息和SRTM DEM生成。卫星轨道信息和SRTM DEM可以生成模拟SAR图像，以帮助寻找地面控制点来量化地图几何与之前生成的查找表之间的偏移。通过SAR图像和对应的模拟SAR图像控制点之间的相关匹配确定这种偏移量，以此改善查找表，实现SAR图像从斜距坐标到地距离坐标的转换。

地形起伏区域的SAR模拟图像与真实SAR图像十分相似(图1)，适合选取控制点；而在地形平坦区域， SAR模拟图像无法提供任何有利于选取匹配控制点的几何特征(图2)。图2(c)为对应的TM红波段图像，其与SAR图像具有很多共同专题特征，如居民地、道路、农田和水体，参照这些专题特征可以选取控制点。在这种情况下，可用光学图像替代由DEM模拟的SAR图像进行地理编码。

我们采用图3所示的ASAR图像地理编码方法。(1)根据元数据和SRTM DEM生成模拟图像。(2)利用图像相关匹配技术在ASAR图像和模拟图像之间寻找匹配控制点。(3)对匹配结果进行评估：若控制点数

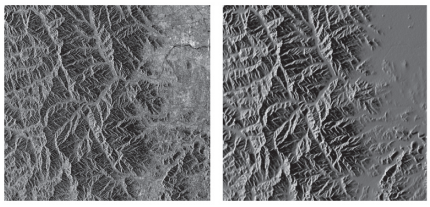

(a) SAR图像 (b) 模拟图像

图1 山区

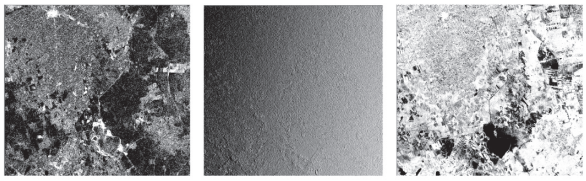

(a) SAR图像 (b) 模拟图像 (c) TM图像

图2 平坦地区图像

不足20个，或者匹配标准差大于0.4(亚像元)，则用TM图像代替模拟图像重新匹配寻找控制点。(4)基于控制点的偏移估计进行二次多项式拟合，生成SAR几何空间和地图几何空间的转换查找表，实现地理编码。采用GAMMA雷达图像处理软件和Unix脚本实现了处理的自动化。

所有的SAR图像被编码到基于WGS84椭球的阿尔伯斯等积圆锥投影系统下。投影的中央经线为东经130°，两条标准投影平行线为北纬25°和北纬47°，采样间隔为50 m。

图4是经过预处理后东北地区的ASAR彩色合成图像。体散射是森林区别于其他地物的主要特征；森林的高HV极化后向散射系数使其在图4上显绿色。

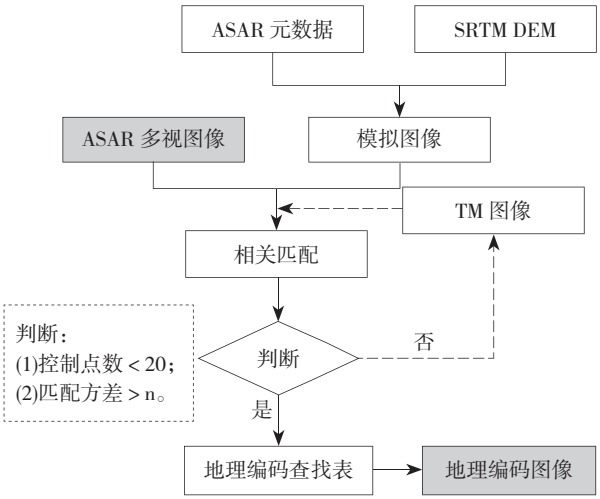


图3 ASAR图像地理编码流程

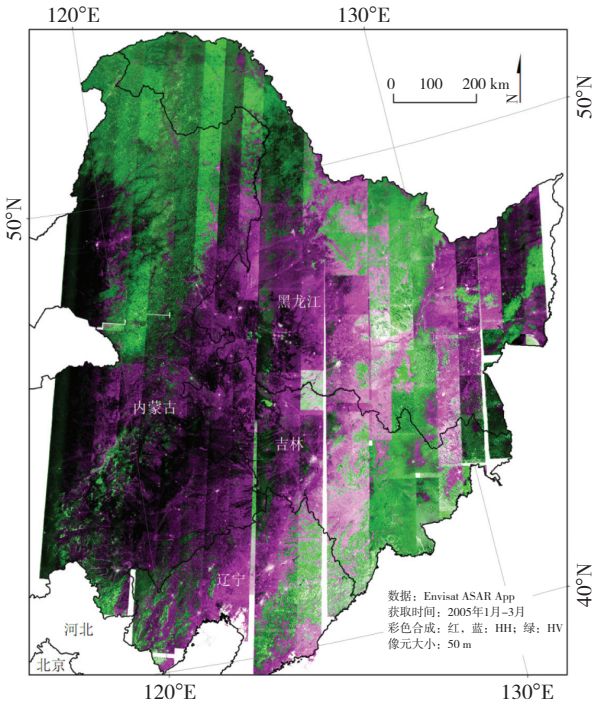


图4 东北ENVISAT ASAR彩色合成图(数据获取于2005年1月—2005年3月；红、蓝：HH极化；绿：HV极化)

## 4 森林–非森林分类

用于分类的数据和数据特征(或称波段)的选择直接影响分类精度。我们在制定分类方法前对数据进行了分析，确定单时相ASAR数据森林-非森林分类的最佳数据获取时间和参与分类的最佳数据特征。在此基础上提出面向对象的分层分类方法，采用eCognition软件实现分类的自动化处理。

### 4.1 数据特征分析

由ENVISAT ASAR的HH和HV两个极化波段可以衍生出纹理、极化比值和图像分割后对象的几何特征、相互关系等数据特征。先利用eCognition软件提供的特征空间优化工具对图像对象的数百个特征进行评价，再进行目视判别。我们认为极化比值和HV极化图像是最佳特征。

大部分研究数据获取于两个时期：(1)夏季(2004年7月—10月)；(2)冬季(2004年12月—2005年3月)。图5是夏季与冬季ASAR图像比较的例子。气温低于0℃、无农作物生长和冰雪覆盖是东北地区冬季环境条件的主要特征。森林和非森林在冬季的强度比值图像上具有最强的对比度，比值图像是最佳区分特征。相反，由于降雨引起土壤湿度增加和农作物的生长，森林和非森林在夏季图像上对比度较弱。图5显示了大部分农田呈现和森林相似的特征。森林和非森林在冬季的HV图像(图5(f))上比在夏季的HV图像(图5(b))上具有更强的对比度。在夏季彩色合成图像(图5(d))上森林和农作物都显绿色，而在冬季图像上(图5(h))只有森林显绿色。

以图5所示区域为例，通过典型地物的直方图分析来比较HH、HV和比值图像对森林的识别能力(图6)。从图6(a)、(c)和(e)可见，夏季的3个特征都无法将森林和农作物区分。冬季的极化比值(图6(f))对森林和农作物的区分度最大。湖泊和河流等水体在夏季对雷达波产生镜面反射，后向散射在HH和HV极化上都很低，容易区分。而在冬季，水体被冰雪覆盖，表面粗糙度增加，以及雪的体散射使得这些区域形成强的后向散射，HH和HV后向散射与森林相当，但极化比值能区分。

通过目视比较和直方图分析可知：冬季数据比夏

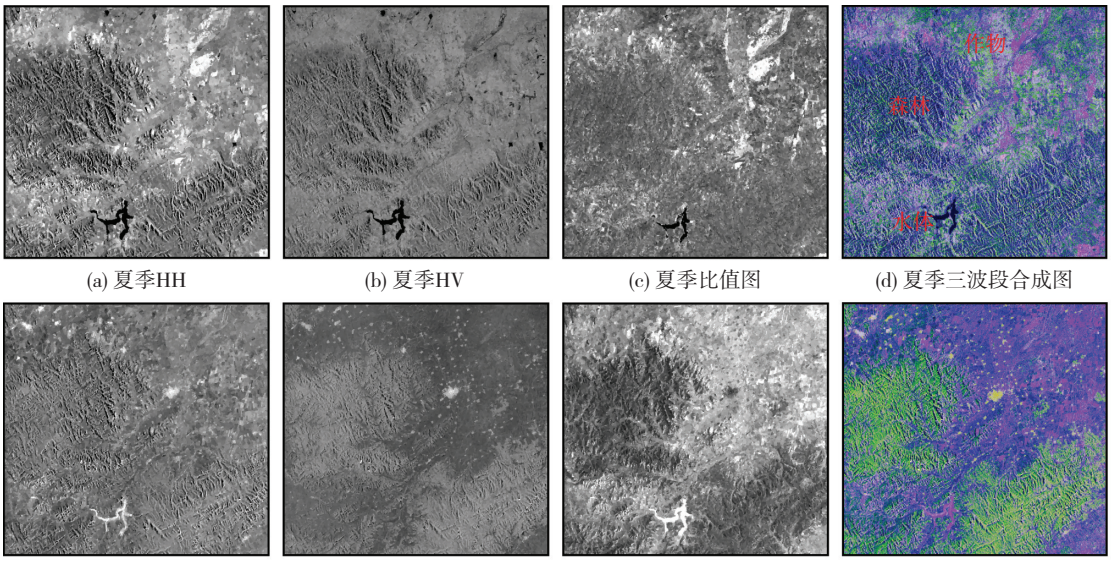


(a) 夏季HH (b) 夏季HV (c) 夏季比值图 (d) 夏季三波段合成图

(e) 冬季HH (f) 冬季HV (g) 冬季比值图 (h) 季三波段合成图

图5 夏季与冬季ASAR图像比较(夏季：2004-09-04;冬季：2005-02-26)
(红：HH极化；绿：HV极化；蓝：比值)

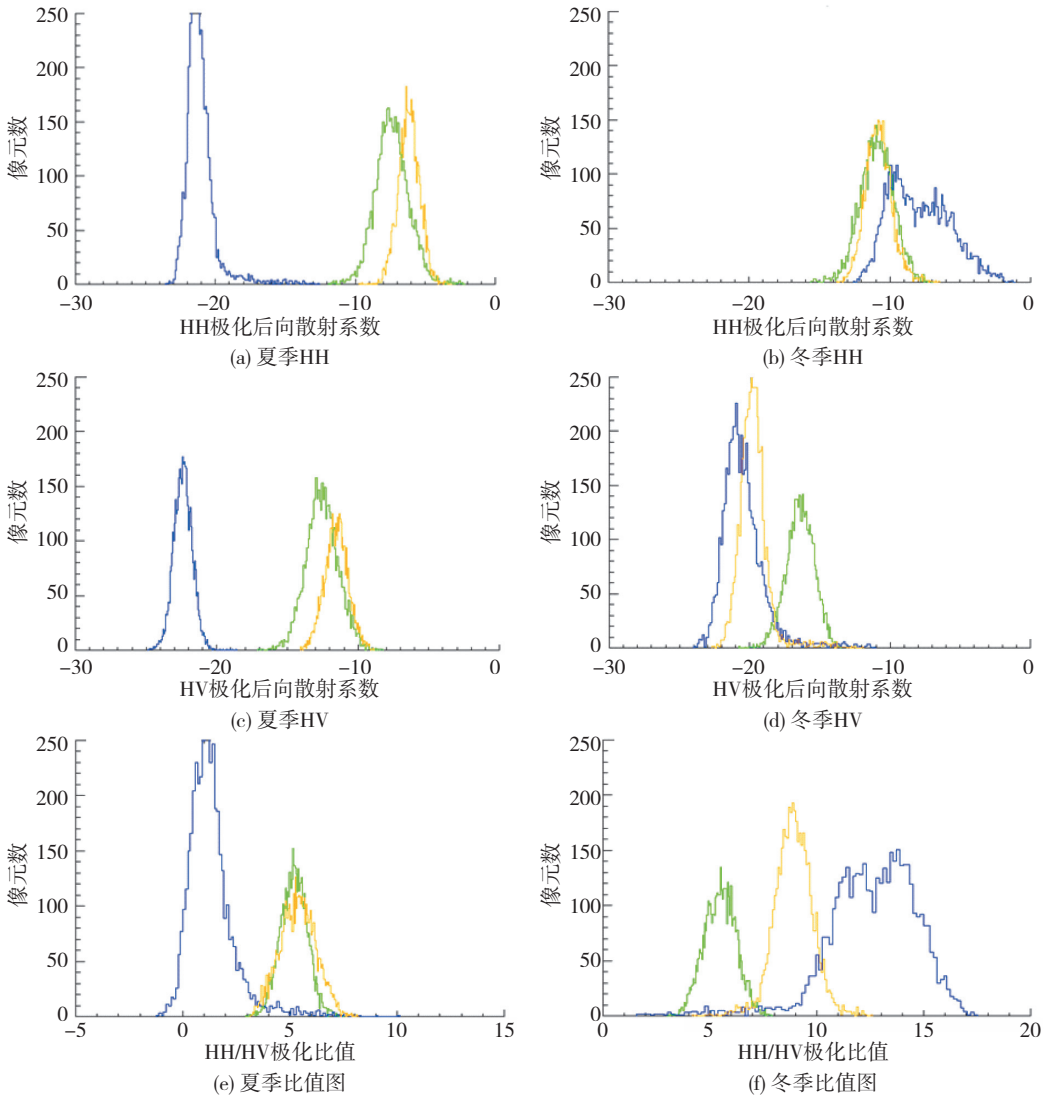


图6 典型地物直方图比较(夏季：2004-09-04；冬季：2005-02-26)

季数据更适合森林–非森林分类；极化比值图像的森林-非森林区分能力强于HV极化和HH极化图像。此外，我们发现某些植被类型(如内蒙古境内的高盖度草地)与森林都具有很低的极化比值。而这些植被类型的HV极化值较低，与森林不同。因此，我们最终选择冬季(2005年1月—3月)的极化比值和HV极化后向散射值作为分类的输入。

### 4.2 面向对象分类

基于极化比值和HV图像在eCognition软件中实现面向对象的分层分类。分类结构如图7所示，包括图像分割、基于对象分类和分类结果优化3个步骤。

首先，采用多分辨率分割方法(Benz 等，2004)进行分割。3个主要参数决定该分割方法的结果：尺度参数、颜色参数和形状参数。尺度参数限定分割对象内部的最大异质性；尺度参数越大，分割对象越大。颜色参数和形状参数进而确定在某一尺度下分割对象的均质性。通常，颜色参数比尺度参数更重要。本研究分割目标是得到尽可能大且均质的图像对象。通过比较不同参数，最终确定分割尺度为10，颜色和形状参数分别为0.9和0.1。

其次，基于图像分割的对象进行分层分类。基于对象分类不仅能利用图像本身的像元值信息，而且能利用对象之间的关系。(1)区分图像区域和非图像区域，这些区域的HV极化值为0。类间关系被用来对“图像区域”分类，即未归类于“背景”的对象被分为“图像区域”类。(2)利用类的继承关系在“图像区域”的对象内区分森林和非森林对象。利用“森林”的极化比值和HV极化后向散射的动态范围对“森林”类制定分类规则。同样，利用类间关系将未被分为“森林”的对象归为“非森林”。由于数据获取的时间不同，图7中森林规则的阈值根据不同成像轨道数据的特征稍有不同。

最后，利用分类后对象的相邻关系对分类结果进行优化。初始分类结果包含很多零星分布的对象，例如少数“非森林”对象被成片的“森林”对象包围，或者相反的情况。引起这种现象的原因有两点：(1)地形引起的辐射畸变无法通过预处理完全纠正，使得某些“森林”像元被分类为“非森林”；(2)在非森林区域，零散分布的树木和其他植被的后向散射特征与森林相似。我们利用对象之间的相邻关系对分类结果进行优化：(1)当一个“非森林”对象的边缘超过80%部分与“森林”对象相邻时，将其重新分类为“森林”；(2)当一个“森林”对象的边缘超过80%部分与“非森林”对象相邻时，将其重新分类为“非森林”。利用对象间的相邻关系对分类结果优化，不仅使零星分布的对象得以合并，而且还实现了对透视收缩、雷达阴影区域对象的分类。图7所列操作过程通过eCognition软件的处理树功能实现了自动化处理。

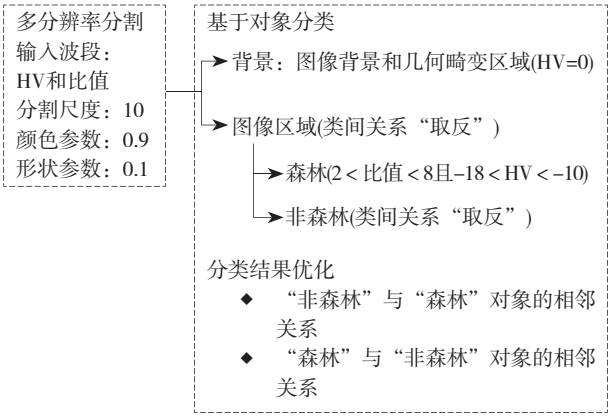


图7 面向对象的ASAR图像森林-非森林分类流程

## 5 结果与误差分析

### 5.1 分类结果

图8是根据本文的预处理和分类方法得到了东北地区2005年的森林-非森林分布图。表1是参考Landsat TM土地利用图的精度验证结果。我们采用基于混淆矩阵的精度验证方法 (Congalton, 1991；Foody，2002)。Kappa系数能指示分类过程的随机性。总体精度由正确分类像元数与图像像元总数相除得到。生产者精度由某一类正确分类像元数与参考图像中该类像元总数相除得到；漏分误差越大，生产者精度越低。用户精度由由某一类正确分类像元数与分类图中该类像元总数相除得到；多分误差越大，用户精度越低。

**表1 基于ENVISAT ASAR的东北森林-非森林分类精度**

| Kappa系数 | 总体精度 | 森林用户精度 | 森林生产者精度 | 非森林用户精度 | 非森林生产者精度 |
|---|---|---|---|---|---|
| 0.67 | 83.7% | 85.6% | 75.7% | 82.6% | 90% |

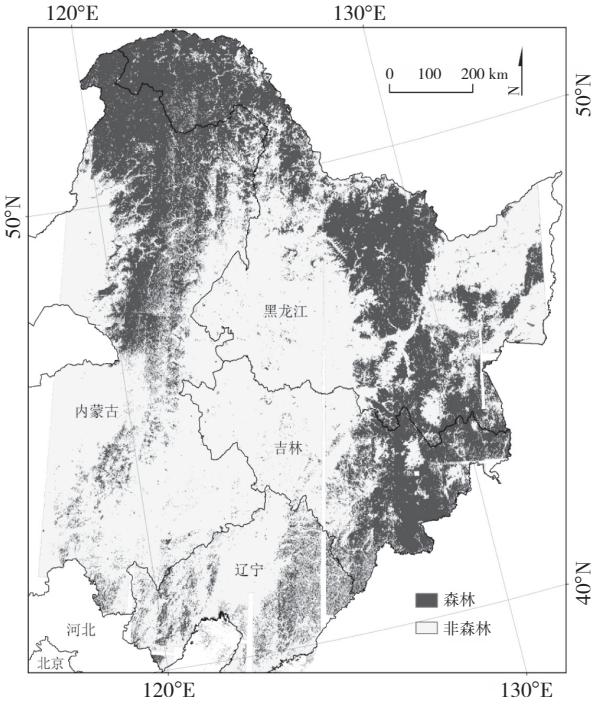


图8 基于ENVISAT ASAR的东北森林-非森林分布图

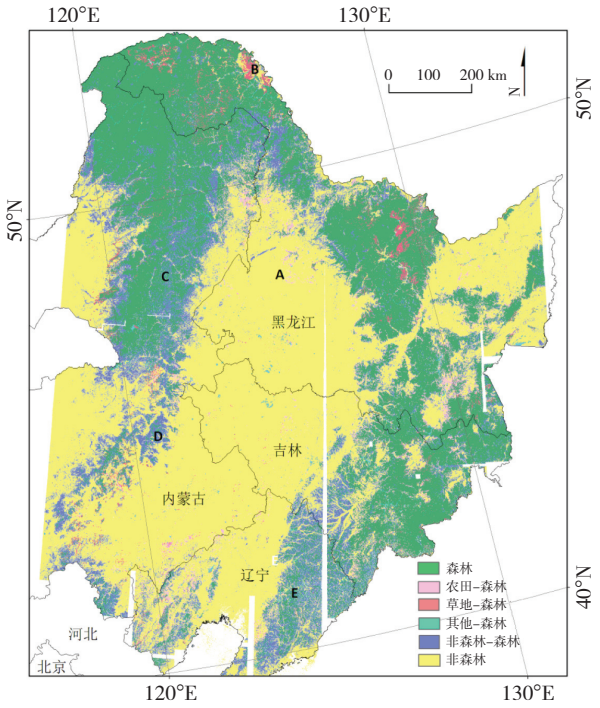


图9 森林-非森林分类误差图

### 5.2 误差分析

东北地区地域辽阔，图像覆盖区域的地形、地貌各具差异，数据获取时间不同，成像期间的气象条件不一。这些环境因素的差异给应用相同的方法对所有图像分类带来了困难。图9是根据类别合并后的TM土地利用图生成的分类误差图。由图9可见，引起森林“多分”的地类主要为农田和草地。例如，在图9“A”所示农业区出现了误分，这是由于林木苗圃表现出与森林类似的特征所致。复杂的结构引起雷达波与之发生多次反射(或称体散射)，形成较强的交叉极化后向散射，致使该地的极化比值和HV后向散射特征与森林一致，引起分类误差。图9“B”所示区域在2003年发生了森林大火，经过自然恢复2005年为草地。但在某些过火区，由于火烧后残留的树木，致使这类区域被误分为森林。另一种分类误差表现为“少分”，即森林被误分为非森林。从图9上大量分布的蓝色区域可见，“少分”现象是引起分类精度降低的主要误差，这与表1中森林的生产者精度较低一致。“少分”误差主要来自地形的影响。对照DEM分析可知，地形起伏较大区域出现较多“少分”现象。图9“C”处出现沿着方位向规则分布的蓝色条带，这是由于地形和当地入射角的影响，造成同一幅SAR图像上近距端比远距端分类精度低。图9“D”和“E”处地形起伏较大，地块相对破碎，同样出现了较为严重的“少分”现象。

参考图像(2005年TM分类图)的精度是引起制图精度评定结果降低的另一原因。例如，我们在2011年9月对漠河县的考察表明：TM分类图所示的“草地”类部分已经恢复成林地。参考图像存在错误，SAR图像分类结果在这些区域更为准确。

## 6 结 论

基于ENVISAT ASAR HH/HV模式数据，提出了SAR图像预处理的自动化方法和面向对象的森林-非森林分类方法。应用于中国东北地区森林-非森林制图，取得了令人满意的结果。本文的方法对及时、准确地开展区域森林-非森林制图十分有效。

### 参考文献(References)

Baker J, Balzter H, Davidson M, Eriksson L, Gaveau D, Gluck M, Holz A, Luckman A, Marschalk U, McCallum I, Nilsson S, Öskog A, Quegan S, Rauste Y, Roth A, Schmullius C, Shvidenko A, Tansey K, Le Toan T, Vietmeier J, Wagner W, Wegmüller U, Wiesmann A and Yu J J. 2001. SAR Imaging for Boreal Ecology and Radar Interferometry-Final report. [2011-05-02] http://www.siberia1.uni-jena.de/

Benz U C, Hofmann P, Willhauck G, Langenfelder I and Heynen M. 2004. Multi-resolution, object-oriented fuzzy analysis of remote sensing data for GIS-ready information. ISPRS Journal of Photogrammetry and Remote Sensing, 58(3/4): 239–258 [DOI: 10.1016/j.isprsjprs.2003.10.002]

Cartus O, Santoro M, Schmullius C and Li Z Y. 2011. Large area forest stem volume mapping in the boreal zone using synergy of ERS-1/2 tandem coherence and MODIS vegetation continuous fields. Remote Sensing of Environment, 115(3): 931–943 [DOI: 10.1016/j.rse.2010.12.003]

Congalton R G. 1991. A review of assessing the accuracy of classifications of remotely sensed data. Remote Sensing of Environment, 37(1): 35–46 [DOI: 10.1016/0034-4257(91)90048-B]

De Grandi G, Mayaux P, Rauste Y, Rosenqvist A, Simard M and Saatchi S S. 2000. The Global Rain Forest Mapping Project JERS-1 radar mosaic of tropical Africa: development and product characterization aspects. IEEE Transactions on Geoscience and Remote Sensing, 38(5): 2218–2233 [DOI: 10.1109/36.868880]

Foody G M. 2002. Status of land cover classification accuracy assessment. Remote Sensing of Environment, 80(1): 185–201 [DOI: 10.1016/S0034-4257(01)00295-4]

Henderson F M and Lewis A J. 1998. Principles and Applications of Imaging Radar, Manual of Remote Sensing, Third Edition, Volume 2. Toronto: ASPRS, John Wiley and Sons Inc

Lee J S. 1980. Digital image enhancement and noise filtering by use of local statistics. IEEE Transactions on Pattern Analysis and Machine Intelligence, 2 (2): 165–168

Quegan S and Yu J J. 2001. Filtering of multichannel SAR images. IEEE Transactions on Geoscience and Remote Sensing, 39(11): 2373–2379 [DOI: 10.1109/36.964973]

Rauste Y. 2005. Multi-temporal JERS SAR data in boreal forest biomass mapping. Remote Sensing of Environment, 97(2): 263–275 [DOI: 10.1016/j.rse.2005.05.002]

Rosenqvist A, Shimada M, Chapman B, McDonald K, De Grandi G, Jonsson H, Williams C, Rauste Y, Nilsson M, Sango D and Matsumoto M. 2004. An overview of the JERS-1 SAR Global Boreal Forest Mapping (GBFM) project. Proceedings of 2004 IEEE International Geoscience and Remote Sensing Symposium, 2: 1033–1036

Schmullius C, Holz A and Vietmeier J. 1999. SIBERIA-results from the IGBP Boreal Forest Transect. Hamburg: Proceedings of IGARSS’99 Conference: 2118–2120 [DOI: 10.1109/IGARSS.1999.775049]

Shimada M, Isoguchi O, Motooka T, Shiraishi T, Mukaida A, Okumura H, Otaki T, Itoh T, Rosenqvist A, Kato A and Sasai T. 2011. Generation of 10 m resolution palsar and jers-sar mosaics and forest/non-forest maps for forest carbon monitoring. Proceedings of ISRSE34, Sydney, Australia

Wagner W, Luckman A, Vietmeier J, Tansey K, Balzter H, Schmullius C, Davidson M, Gaveau D, Gluck M, Le Toan T, Quegan S, Shvidenko A, Wiesmann A and Yu J J. 2003. Large-scale mapping of boreal forest in SIBERIA using ERS tandem coherence and JERS backscatter data. Remote Sensing of Environment, 85(2): 125–144 [DOI: 10.1016/S0034-4257(02)00198-0]

Wegmüller U. 1999. Automated Terrain Corrected SAR Geocoding. Hamburg: Proceedings of IGARSS’99: 1712–1714